EXPERIMENTAL STUDY OF STRONG FIELD IONIZATION AND HIGH HARMONIC GENERATION IN MOLECULES

by

ARAM VAJDI

B. S., Razi University, Iran, 2006
M. S., Kurdistan University, Iran, 2009

A REPORT

Submitted in partial fulfillment of the requirements for the degree

MASTER OF SCIENCE

Department of Physics
College of Arts and Sciences

KANSAS STATE UNIVERSITY
Manhattan, Kansas

2015

Approved by:

Major Professor
Vinod Kumarappan

Copyright

.

Abstract

This report includes the experimental details and results of two experiments. The first experiment addresses carrier envelope phase (CEP) effects in higher order harmonic generation (HHG), and the second experiment is a pump-probe experiment on CO_2 molecules using ultrashort laser pulses.

Ultrashort laser pulses that are only a few optical cycles long are of interest for studying different atomic and molecular processes. The CEP of such a pulse is an important parameter that can affect the experimental results. Because the laser pulses we used in the HHG experiment have random CEP, we tagged a given harmonic spectrum with the CEP of the fundamental laser pulse that generated it by measuring both shot-by-shot. The first chapter of this report is about the experimental details and the results we got from our CEP-tagged HHG experiment that enabled us to observe the interference of different quantum pathways.

In the second experiment, discussed in the second chapter of this report, we tried to study the structure of the CO_2^+ ion created by strong field ionization in a pump-probe experiment. For this experiment, we used an ultrashort laser pulse to ionize CO_2 molecules, and after various time delays we probed the ionic wave packet by ionizing CO_2^+ with another ultrashort laser pulse. By performing Fourier analysis on the delay-dependent CO_2^{++} yield, we were able to identify the populated states of CO_2^+.

Table of Contents

List of Figures

Acknowledgements

I would like to express my gratitude to Professor Vinod Kumarappan. Beside all the physics and technical skills that I learnt from him, he taught me how I should work in a professional science environment.

I would like to thank Varun Makhija and Xiaoming Ren two great senior students. I appreciate the knowledge that I got from them. I appreciate Varun's patience for putting up with me during the beam-times. I want to thank Rajesh Kushawaha our group member and Matthew Rothfuss for all their help and time we spent together. I would like to acknowledge prof. Itzik's group members Mohammad Zohrabi, Ben Berry, Bethany Jochim, and Travis Severt, for all their help during beam-times in Pulsar Lab. I would especially like to thank Bethany Jochim for proofreading this report. I would also like to thank Derrek Wilson for aligning the OPA in KLS Lab which we used for our experiments. I am also grateful for all the technical support I got from Al Rankin, Mike Wells, Scott Chainey and Vince Needham.

Chapter 1 - Phase-tagged Harmonic Generation

1.1 Introduction

For the ultrashort laser pulses that are two or three optical cycles long, the Carrier Envelope Phase (CEP) is an important parameter that can affect experimental results [1]. Higher-order Harmonic Generation (HHG) can be considered as burst of attosecond pulses in each half-cycle of the driving laser pulse and what we detect is the interference of these attosecond pulses. Moreover, the characteristics of these attosecond pulses depend on the electric field of the half-cycle that they are generated in. For the driving laser pulses that contain several optical cycles, for different CEP's the temporal profile of the electric field does not change substantially. On the other hand, for the laser pulses that are two or three optical cycles long, CEP is an important parameter that affects the temporal profile of the electric field, which in turn can affect the characteristics of different half-cycle emissions in the HHG experiments. By obtaining HHG spectra for different CEP's, it is possible to study the individual attosecond pulses [2], which is important because it contains information about the dynamics of atoms and molecules in the attosecond timescale. Moreover, the CEP of the driving laser pulse in HHG can be used as a control knob. In some studies, the spatially-filtered half-cycle cut off in harmonic spectra has been used to generate isolated attosecond pulses or to characterize the ultrashort pulses [3, 4, 5].

1.2 Background

1.2.1 High-order Harmonic Generation

The advent of pulsed lasers with high intensity has enabled researchers to explore some atomic and molecular processes that they were not able to study before. If the laser intensity is

higher than $10^{14}\ \frac{W}{cm^2}$, the interaction of the laser with atoms and molecules is comparable with the Coulomb field and is, therefore, not perturbative. High-order harmonic generation (HHG) [6, 7, 8] is a highly nonlinear process that is an outcome of the interaction of intense laser pulses with a medium. In a typical high-order harmonic generation experiment, an intense laser pulse with frequency ω interacts with a gaseous medium and produces photons of higher energy with frequencies$(2n+1)\omega$. A semiclassical model to explain HHG proposes that this process happens in three steps [6]. First the electric field of a low frequency laser pulse distorts the Coulomb potential, forming a potential barrier through which electrons can tunnel. The parameter that determines the tunneling regime is known as the Keldysh parameter γ

$$\gamma = \sqrt{\frac{I_p}{2U_p}} \tag{1.1}$$

where I_p is the ionization potential and U_p is the ponderomotive energy.

$$U_p = \frac{e^2 {E_0}^2}{4m_e {\omega_0}^2} \tag{1.2}$$

.

If $\gamma \ll 1$ the atomic system is tunnel ionized. For $\gamma \gg 1$ ionization is in the multiphoton regime. After tunnel ionization, the second step in the semiclassical model is propagation, where the electron is considered to be no longer interacting with the Coulomb field of the parent ion. When the electric field changes direction, the electron is driven back to the parent ion by the laser electric field. The returning electron is then recombined with the parent

ion and photon that has energy equal to the ionization potential plus the kinetic energy of the recombining electron is generated. The maximum energy that an electron can acquire through propagation in the laser electric field is $3.17U_p$. So the maximum energy of generated photons is I_p+$3.17U_p$ which defines the classical cutoff energy for the emitted harmonic photons.

1.2.2 Carrier Envelope Phase

The temporal profile of an ultrashort Gaussian laser pulse can be written as

$$E(t) = E_0\, e^{-\frac{t^2}{\tau^2}} \cos(\omega t + \varphi) \tag{1.3}$$

where φ is the called carrier-envelope phase (CEP) of the laser pulse. In our experiment, the goal was to study the effect of CEP on harmonic spectrum. In order to understand the results of our experiment, the general theory proposed in ref. [9] is adopted. Starting from the time- dependent Schrödinger equation, it was shown in ref. [9] that the CEP dependent wave function can be obtained as

$$\Psi(\varphi; t) = \sum_{n=-\infty}^{\infty} e^{in\varphi} e^{in\omega t} \phi_n(0; t) \tag{1.4}$$

where $\phi_n(0; t)$ is obtained from solving Schrödinger equation for $\varphi = 0$. Moreover, $\phi_n(0; t)$'s can be interpreted as the amplitude of the n-photon channels. If two or more $\phi_n(0; t)$ in the expansion of the wave function are non-zero, we should observe interference between them, which leads to different Fourier components in the measured observable.

1.3 Experimental Setup

1.3.1 Laser System

The laser system used for phase-tagged harmonic generation is the PULSAR laser located in the JRM Lab. PULSAR is a femtosecond laser that includes an oscillator, which produces pulses with a repetition rate of 75 MHz and pulse energy of 4 nJ. The central frequency of these pulses is 780 nm, and the pulse duration is 14 fs. The output of the oscillator is sent to a stretcher and two-stage amplifier to get amplified pulses by the chirped pulse amplification process (CPA). After amplification, the laser pulses go through a compressor, outputting 2 mJ pulses at 10 kHz repetition rate with pulse duration of 21 fs at a central wavelength of 790 nm [10].

1.3.2 PULSAR Hollow-core Fiber

For our experiment, we used 0.9 mJ output of the PULSAR as the input to a hollow-core fiber located in the PULSAR lab. The fiber was filled with Neon gas at 2 bar, and the pulse duration of the fiber output was less than 7 fs. Details about the fiber system can be found in reference [10]. The spectral broadening in the fiber is the result of self-phase modulation, which is a third order nonlinear effect that leads to intensity-dependent modulation of the refractive index of the gas in the fiber. The output of the fiber is sent through a set of chirped mirrors to compensate for the substantial positive chirp acquired during spectral broadening.

1.3.3 HHG Set Up

The harmonic chamber installed in the PULSAR lab had three main parts

a) A source chamber with a capillary tube sealed from one side using vacuum-compatible glue and connected to a gas source from the other side. By focusing laser on the gas tube, it was possible to make a hole of micrometer size through the gas tube, so the laser could interact with the gas inside, and produce harmonic photons.

b) A differential pumping chamber, which was designed to separate the source chamber and detection chamber and maintain low pressure in the detection chamber in order to protect the microchannel plate (MCP) detector from damage. Moreover, a movable silver mirror was installed in the chamber for alignment purposes. By looking at the reflected beam from the silver mirror, we were able to align the beam through the hole drilled through the gas tube.

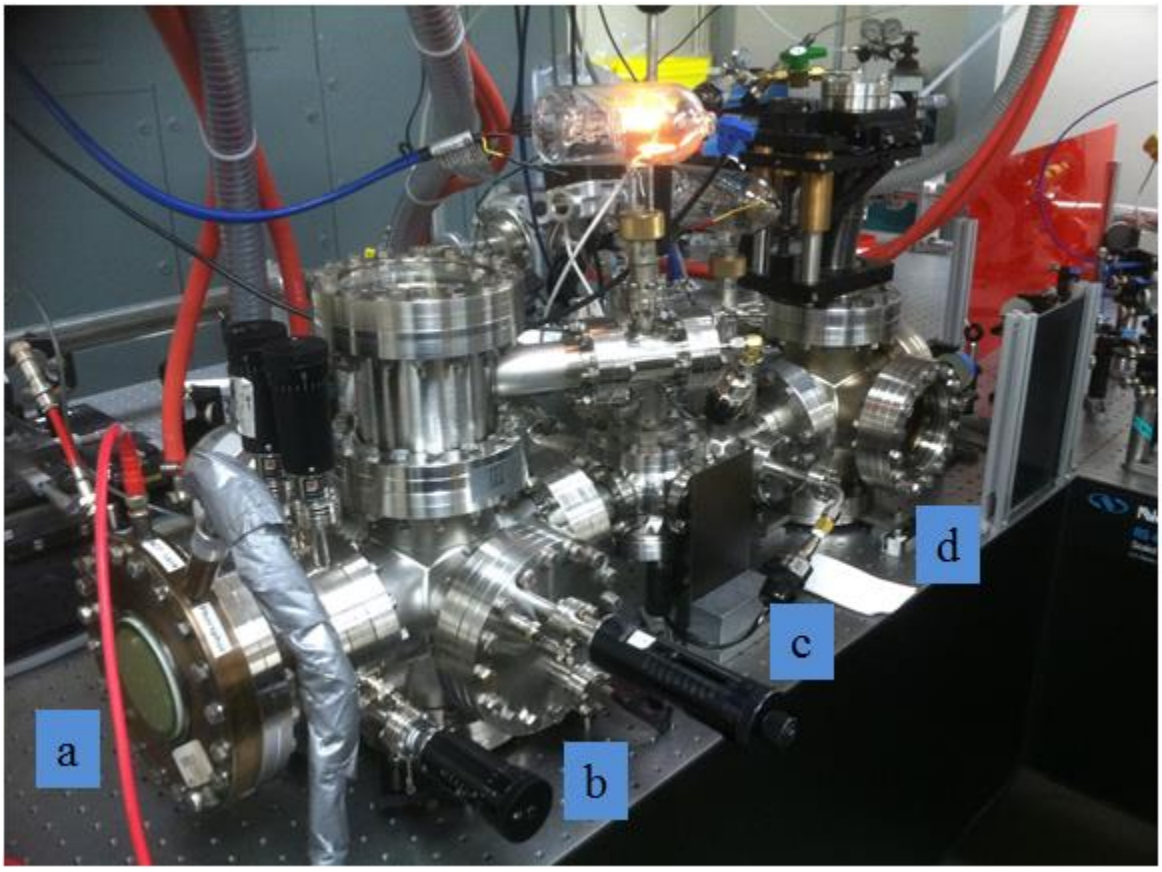

Figure 1.1 Image of the HHG Setup. The MCP (a), detection chamber (b), differential pumping chamber (c), and source chamber (d) are shown in the picture. The beam path in the chamber is shown in Fig. (1.2).

c) In the detection chamber, an aluminum filter of 0.15 micrometer thickness was installed to block the fundamental laser beam and transmit harmonic photons. The purpose of blocking the fundamental laser beam was to prevent the grating from heating up and getting damaged. The grating that was used for separating harmonic photons with different energies was a transmission

nanograting [11]. The other component installed in the detection chamber was a Z-stack MCP with a fast phosphor screen with life time less than 1 microsecond. By using a fast phosphor screen, we were able to detect generated harmonic photons from each laser shot of 10 kHz laser pulses.

1.3.4 Phasemeter

The phasemeter setup installed in PULSAR lab is an instrument that can be used to retrieve the carrier-envelope phase of each laser shot using the asymmetry of the rescattered electrons. The theoretical basis of this instrument and phase retrieval algorithm can be found in the references [12, 13, 10]. This setup has two MCPs on each side of the chamber Fig. (1.2). By focusing ultrashort laser pulses in the chamber we can measure the asymmetry of Xe ATI yield along the polarization of the laser beam. This asymmetry changes with the CEP of the ultrashort pulse, and for the low energy part of the spectrum is roughly sine-like and for the high energy part of the spectrum is cosine-like. This enables us to make a parametric plot which is called phase potato Fig. (1.2). However, retrieving the CEP requires re-binning the phase potato data using the fact that the CEP's of the laser pulses have a uniform distribution over a 2π range [13]. In our experiment we used a data acquisition card (DAQ) to read two voltages generated by the phase meter setup for each laser shot. These voltages correspond to the asymmetry of the low energy and the high energy parts of the ATI spectrum. After running the experiment for three million shots of the laser we were able to make a parametric plot of the asymmetries and find a conversion table for retrieving the CEP of the laser pulses from the phase potato parametric plot using the algorithm mentioned in ref. [13].

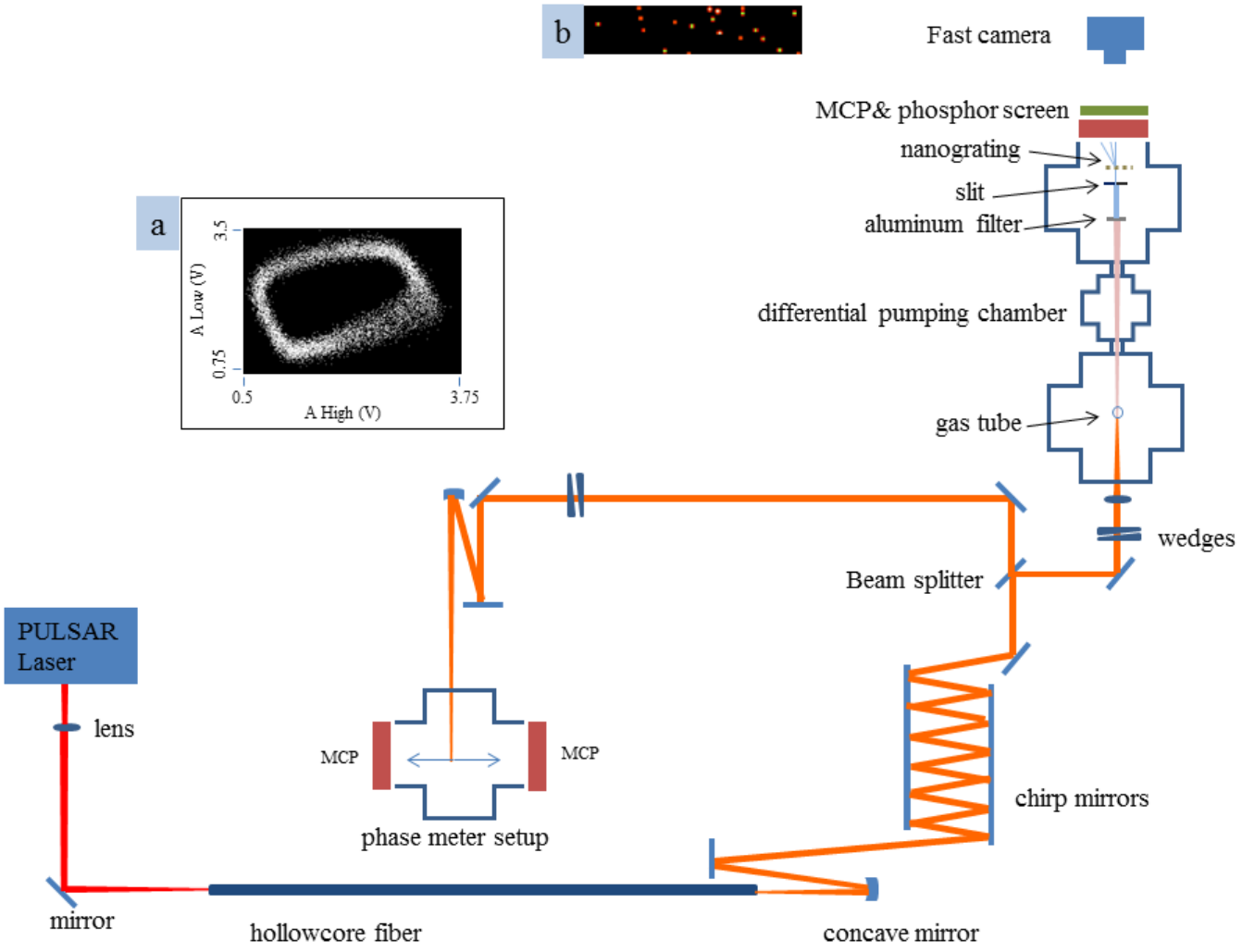

Figure 1.2 Experimental Setup. Parametric plot (a) is the phase potato explaind in the section (1.3.4) and image (b) is the single shot image of the phosphor screen acquired by the fast camera

1.4 Data Acquisition

In this experiment, we tagged generated harmonic spectra with the carrier-envelope phase of the fundamental ultrashort laser pulse. For this purpose we sent some portion of each laser shot to the phase meter setup and let the other portion interact with the gas medium to produce harmonic photons. Data acquisition for the experiment involved two parts. First, for each laser shot, we needed to take an image from the phosphor screen using our camera to figure out what

harmonic photons are produced by the laser pulse. Because the laser pulse repetition rate was 10 kHz and the time interval between successive pulses was 100 microseconds, a fast camera with an exposure of 15 microseconds and a fast phosphor screen were used to run the experiment in single-shot mode. Our imaging program was a LabVIEW program developed by Prof. Kumarappan. In this program, the image information is processed online, and the location of each hit on phosphor screen, corresponding to the detection of a single harmonic photon, is saved in a file. The location of each hit on the phosphor screen tells us the energy of harmonic photon. The details about this program can be found in Xiaoming Ren's PhD thesis [14]. The second part of the acquisition involved reading two voltages from the phasemeter setup. The phasemeter generated 2 voltages for each laser shot that we needed to read in order to retrieve the CEP's of the laser pulses, which were random. In order to achieve this goal we used a pulse generation channel of our camera card to trigger a data acquisition card (DAQ) that was reading the phasemeter signals, and these two signals were saved along with the position of hits in each image. After running the experiment for three million laser shots, the saved file was analyzed, and we were able to reconstruct the phase-tagged harmonic spectra.

The main problem we faced during experiment was local saturation of the MCP, which was due to high density of lower energy harmonic photons on the MCP. After each photon hits a channel on the MCP, the channel is almost dead for a few milliseconds. To avoid this problem we decreased number of generated harmonic photons by decreasing gas density in the interaction region. Moreover, our camera was not fast enough to acquire image at 10 kHz and was dropping the rate to 2 kHz. The timing for data acquisition is shown in Fig. (1.3).

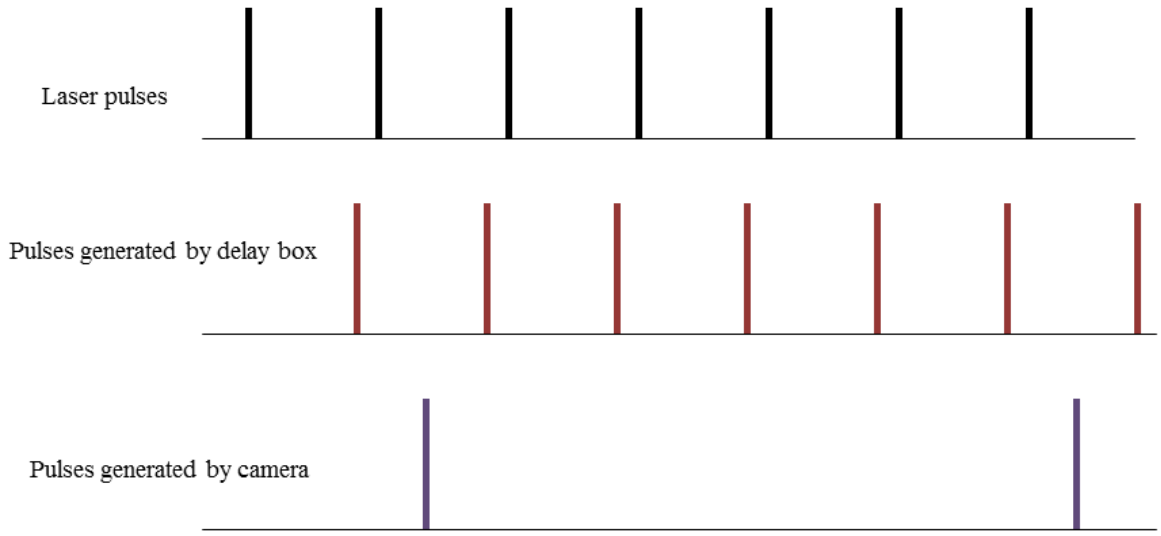

Figure 1.3 Timing of acquisition. 10 kHz laser pulses triggered a delay box, which generated digital pulses with some delay that were used to trigger the camera. The camera was not fast enough to acquire image for each laser pulse, so it was dropping the rate and generating trigger pulses that were sent to a DAQ card.

1.5 Results

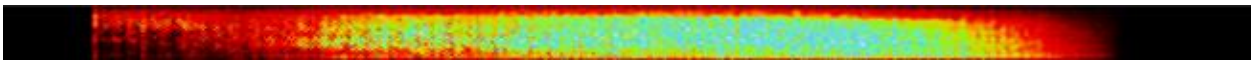

Figure 1.4 Generated harmonic photons from Nitric Oxide

During the experiment, each laser shot was generating few harmonic photons, and we saved the location of them on phosphor screen and constructed an image that includes all the generated harmonic photons. Fig. (1.4) shows all the harmonic photons generated by 3,000,000 laser shots focused in Nitric Oxide gas. The image above does not include CEP dependence, but we had tagged all the photons in Fig. (1.4) with the CEP of fundamental laser pulses. If we plot the

number of photons generated at different energies as a function of CEP we can reconstruct the full CEP dependent spectrum as shown in Fig. (1.5).

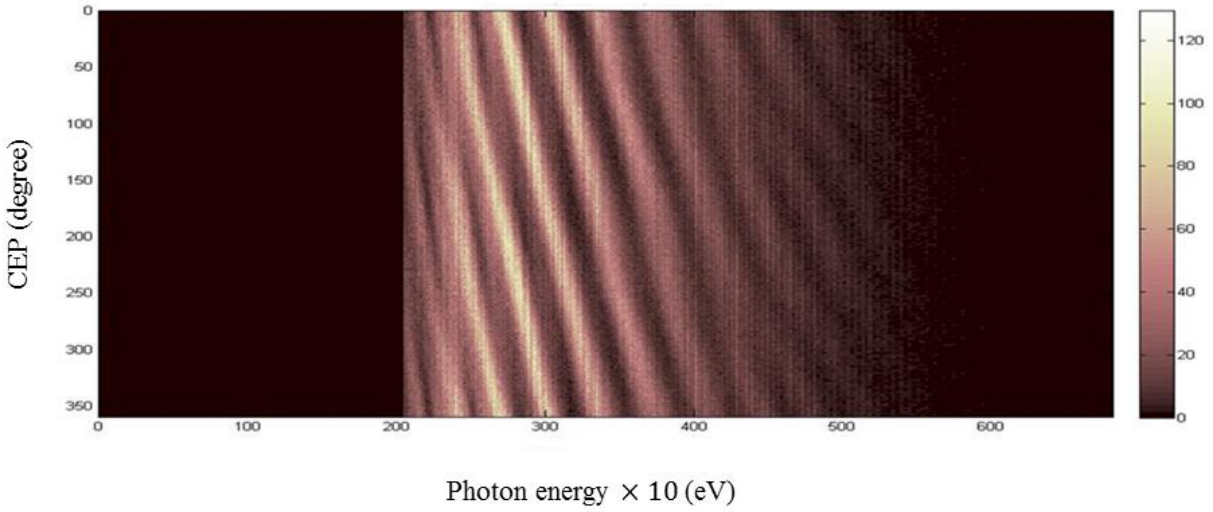

Figure 1.5 After tagging all the harmonic photons with the CEP of the fundamental laser pulses, we can construct the CEP dependence plot of harmonic photons generated from Nitric Oxide.

As expected, the harmonic yield is a periodic function of CEP. Moreover, we are looking at the yield of harmonic photons, so we expect that the periodicity would appear in $\cos n\varphi$ components, where n is an even number. If we integrate the spectrum over a narrow energy range, we can get the CEP dependence for that range of energy. Fast Fourier transforms for three different ranges are shown in Fig. (1.6). In these figures, we can see different regions of energy have different phase periodicity. In the general theory of CEP effects developed by Prof. Esry [9], it is proposed that different Fourier components in the CEP dependence of an observable are results of the interference between different quantum path-ways leading to the same observable. However, quantum pathway interference [9] is not the only picture that we can use to interpret the HHG spectrum. We can consider the HHG spectrum as interference between different half-

cycle bursts of emission with different phases that depend on the half-cycle profile of a driving electric field [15, 6].

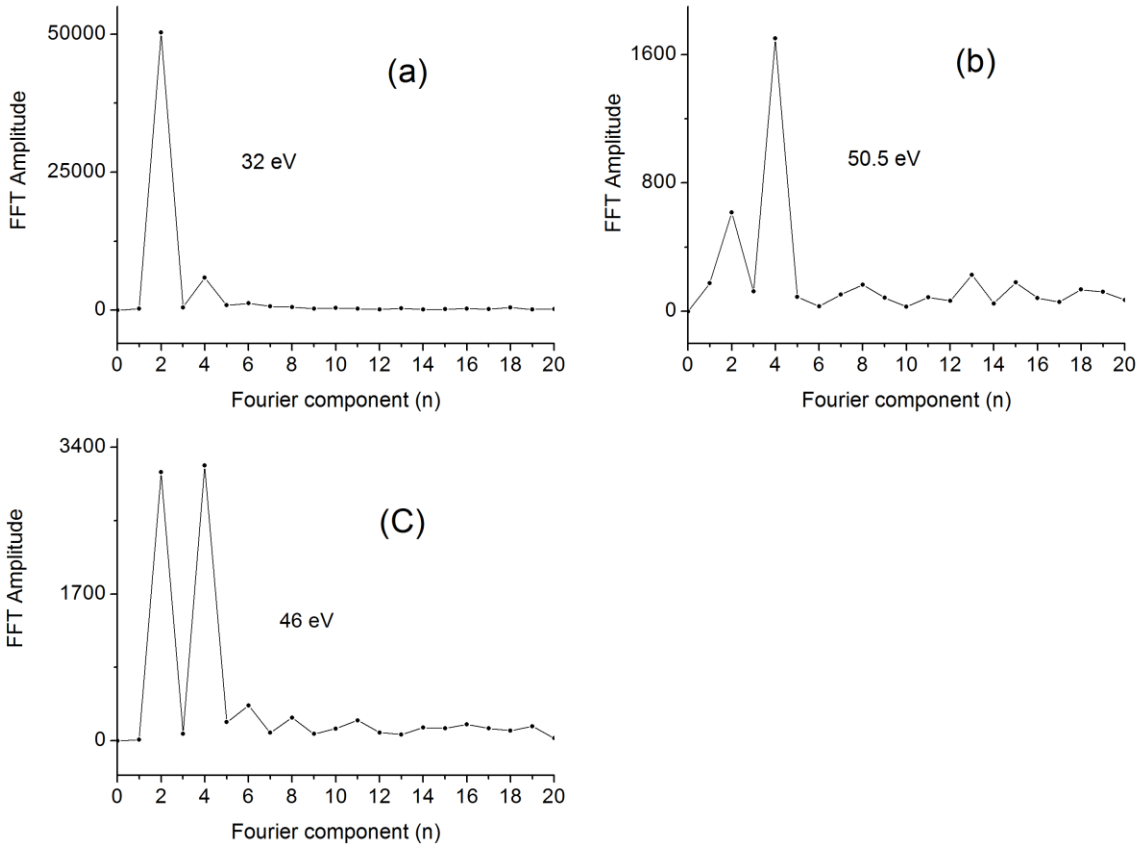

Figure 1.6 CEP periodicity. The graphs show amplitude of different Fourier components for three different photon energy regions in the harmonic spectra shown in Fig (1.5).

1.6 Conclusion

In this experiment we showed that it is possible to use CEP tagging method to study CEP dependence of harmonic spectra generated by the laser pulses with the random CEP's. The important experimental issue was to make sure the data acquisition from the camera and the

phase meter setup are synchronized, which is obvious from the CEP dependence of harmonic spectra shown in Fig (1.5). Moreover, we investigated the general theory of CEP [9]. We saw the harmonic yield is a periodic function of CEP and the periodicity appears in $\cos n\varphi$ components, where n is an even number.

Chapter 2 - Pump probe experiment using ultrashort pulses

2.1 Introduction

Studying charge distributions and their dynamics in molecules and atoms has been one of the motivations for developing ultrafast physics [16]. In order to study the dynamics of electrons after ionization, higher-order harmonic generation has been proposed as a promising method. In principle, harmonic emission happens on the time-scale that the electronic wave packet of the parent ion is evolving, and thus it can be expected that the harmonic spectra contain "finger prints'' of these electronic dynamics. For example, by studying the HHG spectra it has been shown that the electronic state of the parent ion is superposition of different ionic states [17, 18].

In this experiment our goal was to study the wave packet of a molecular system after being ionized. This experiment was performed before using different apparatus [19]. For this experiment, we used an ultrashort laser pulse to ionize target CO_2 molecules and later on we probed the resulting CO_2^+ ions with another ultrashort laser pulse at different time delays.

2.2 Experimental Setup

2.2.1 Laser System

For this experiment we used the KLS laser located in the JRM lab for generating ultrashort laser pulses. KLS generates pulses at a rate of 2 kHz with 2 mJ energy, 790 nm central wavelength, and 30 fs pulse duration. 1mJ of KLS output was focused in the KLS hollow-core fiber in order to generate ultrashort pulses of 7 fs duration through spectral broadening.

2.2.2 VMI

In this experiment, we used a thick lens velocity-map-imaging (VMI) setup [20] that was initially designed for detection of high energy electrons. We modified the original design of the

VMI by removing the first extractor plate in order to make space for the laser beam which was focused in the interaction region using a concave mirror installed in the vacuum chamber Fig. (2.3). The SIMION simulation shows with 16.2 kV on the repeller plate it is possible to focus electrons up to 150 eV on the detector. However, because of insulation problem we need to use thicker ceramic insulators to reach this goal.

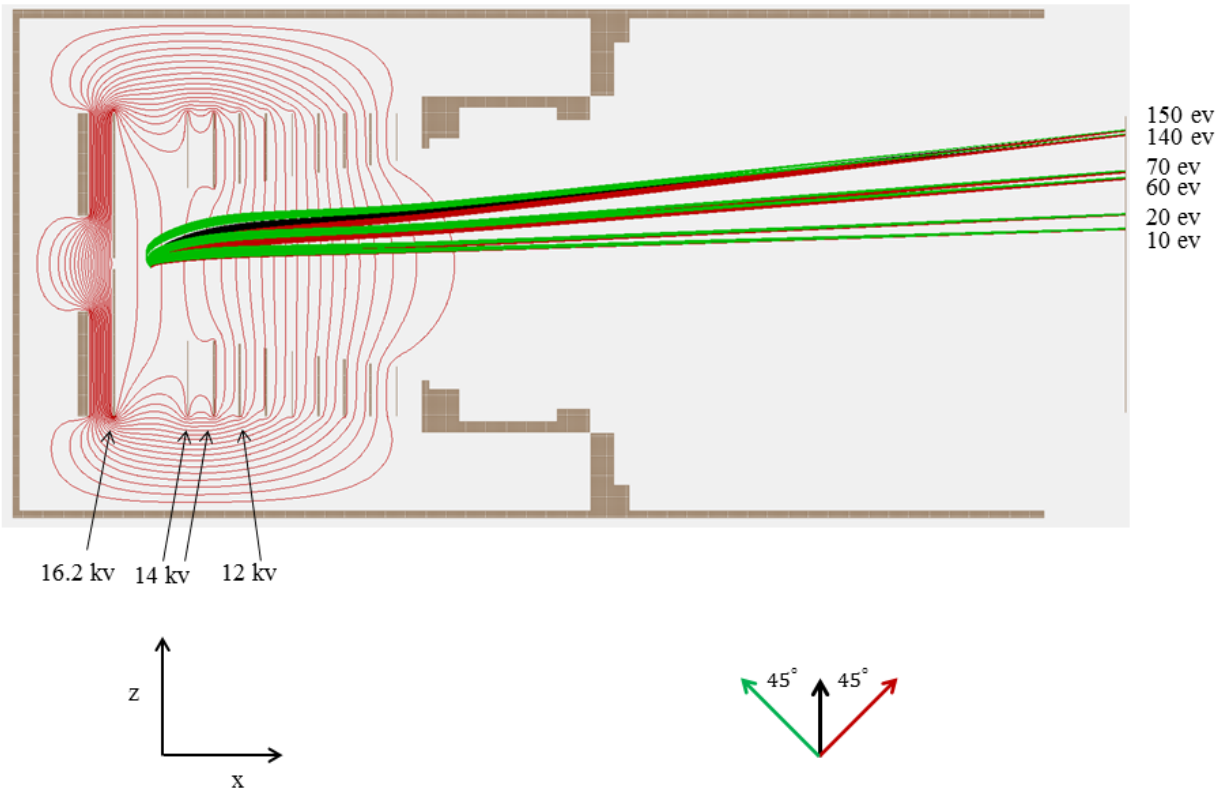

Figure 2.1 SIMION simulation of trajectories for electrons with different energies.

An operational VMI is supposed to focus all the particles that have the same velocity in the Z direction, as shown in Fig (2.1), to the same point on the detector. In the SIMION simulation we defined three groups of particles, shown by red, black and green colors in Fig.

(2.1). These groups of particles have the same velocity in the Z direction but different velocities in the X direction. By changing the voltages on the VMI plates we tried to find an optimum electrostatic field that focuses the three groups of particles to the same place on the detector. In Fig (2.1) the specified energy is the energy of particles that have initial velocity in the Z direction. For the energy calibration of the VMI, we need to use the formula $E = c\,R^2$ where E is the energy of the detected particles, R is the radius of the focal circle on the detector, and c is a constant. We can find out the constant c by looking at different above-threshold ionization (ATI) peaks that are separated by one photon energy. For the particles shown in Fig (2.1), we can plot energy as a function of focal position on the detector. We can see that it follows $E = c\,R^2$ where c is a constant.

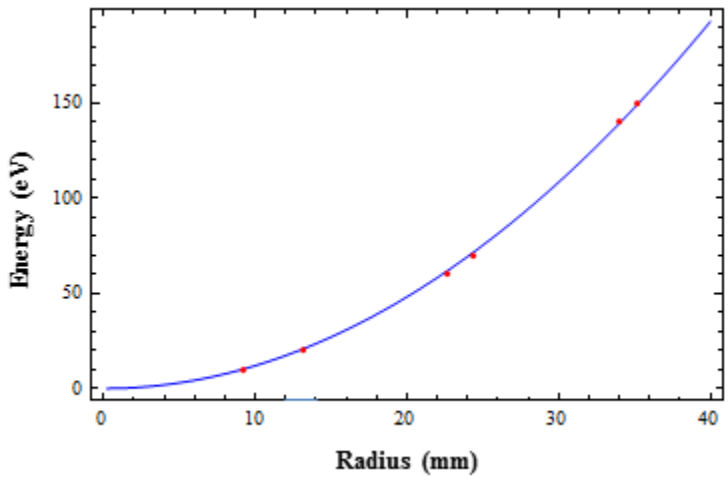

Figure 2.2 Calibration of our VMI. The red data points are the six different electron energies from Fig (2.1), and blue curve follows $E = c\,R^2$ where $c = 0.118$ when 16.2 kV applied on the repeller plate.

2.2.3 Optical Setup

The generated 7 fs laser pulse from the hollow-core fiber was split in to two portions by a

50/50 broadband beam splitter and then recombined collinearly using another 50/50 beam splitter. The portion of the beam that was used as a probe was reflected from a pair of mirrors installed on a translational stage could be moved in 0.5 micrometer steps in order to produce

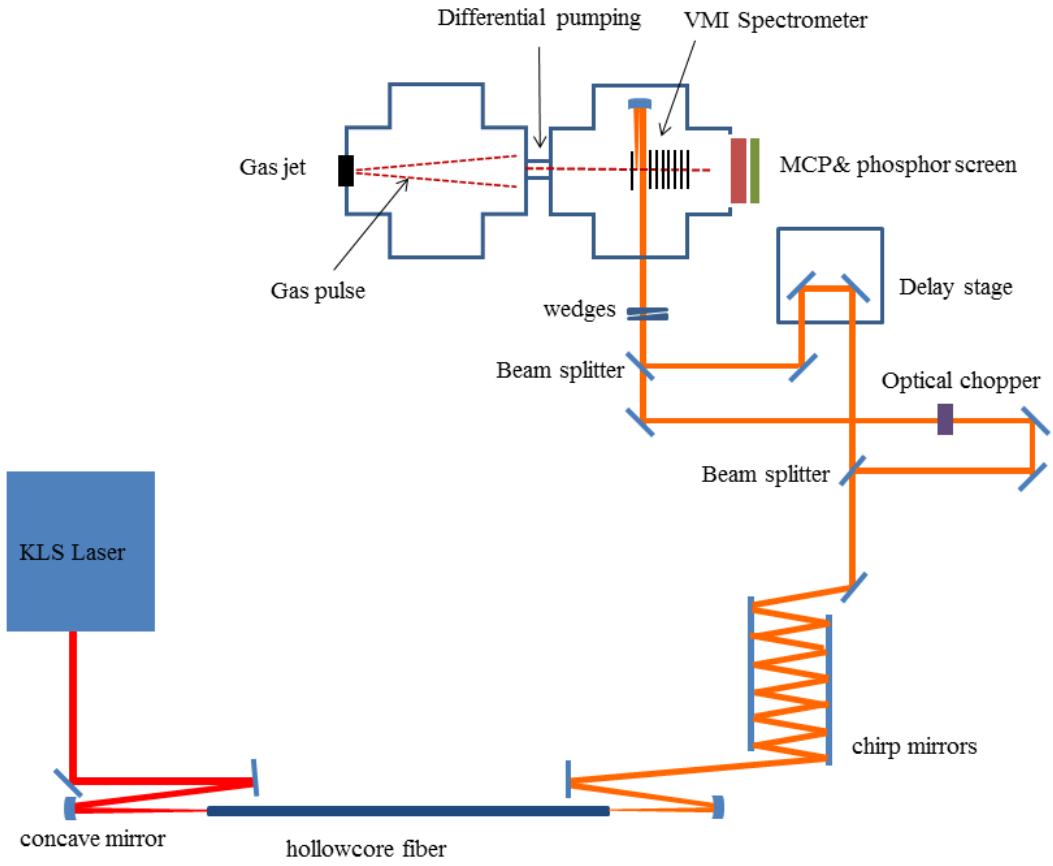

Figure 2.3 Experimental Setup

delay steps of 3.3 fs between the pump and probe pulses. In order to get spatial overlap in the interaction region in the chamber, after recombination we sent both beams into the far field and verified that they stayed collinear. Then, we focused both beams in the interaction region using a focusing mirror installed in the chamber. For finding the time overlap, we changed the delay between pump and probe and looked for the interference pattern on a screen outside the chamber. For fine tuning of the overlap inside the chamber we maximized the ion yield signal from the

MCP. Moreover, to get transform-limited pulses in the interaction region we used a pair of fused-silica wedges and maximized the ion yield by changing the amount of glass in the beam path.

2.3 Data Acquisition

In this experiment, we measured the yield of CO_2^{++} ions using the phosphor screen attached to the back of the MCP as a function of delay between pump and probe. 2 kHz ultrashort probe pulses were interacting with the gas beam from a supersonic gas jet. The details about this gas jet can be found in Varun Makhija's PhD thesis [21]. The produced CO_2^{++} ions were directed toward the MCP using the VMI electrostatic plates. The VMI was not operated at space focusing condition to avoid local saturation of the MCP. The CO_2^{++} ions hitting the MCP produced light on the phosphor screen. To measure the CO_2^{++} ion yield, we gated the MCP in such a way that it was only active at the arrival time of the CO_2^{++} ions. Moreover, we used a fast camera to take an image of the phosphor screen for each probe pulse, and the total yield of CO_2^{++} was measured by adding up values of the pixels in the image. In order to see the effect of the pump pulses on the CO_2^{++} yield, we ran in two different situations:

a. The pump pulse is present before the probe pulse.
b. There is no pump pulse, and the ions are just the result of the interaction of the probe with the CO_2 gas.

For this purpose, we used an optical chopper to block two successive pump pulses and let the next two successive pump pulses interact with the CO_2 molecules. To figure out if the pump pulse was present before the probe pulse, we used a DAQ card to read a digital signal from the optical chopper controller. If the signal was high, the pump pulse was present, and if it was low, the pump pulse was blocked. The important issue was to make sure that the reading of the digital

signal from the DAQ card was synchronized with the camera. To achieve this goal, we triggered the DAQ card with the camera at the start of each exposure time. Moreover, our gas jet runs at 1 kHz repetition rate but the laser repetition rate was 2 kHz. For this reason we used a 1 kHz digital signal, which was generated by the delay box that was triggering our gas jet, to find out if the image was acquired when the gas pulse was present or not.

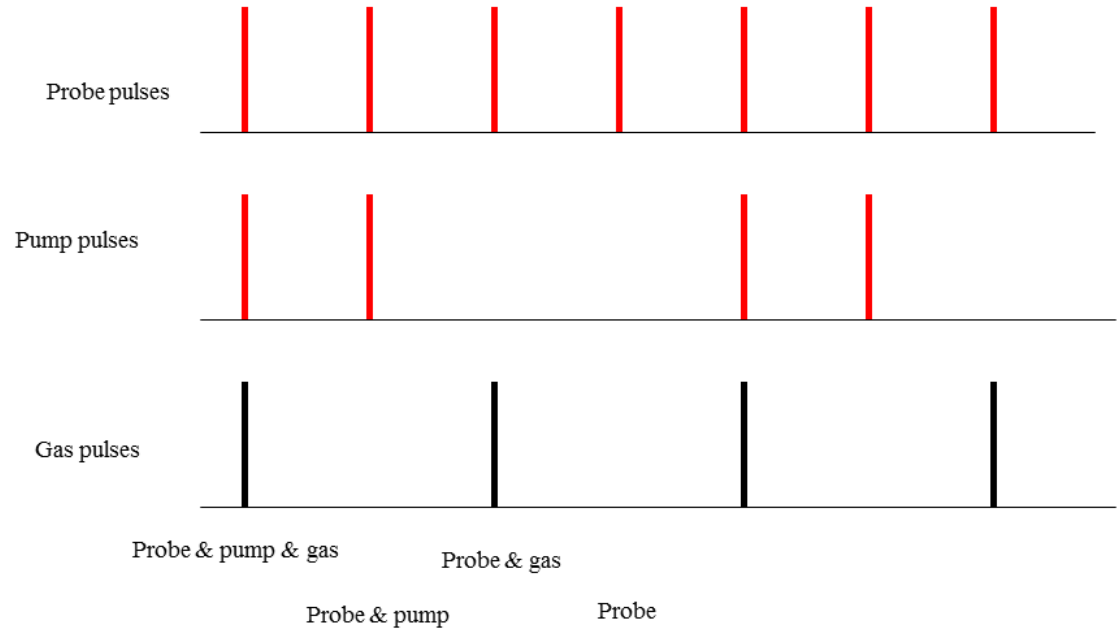

Figure 2.4 Timing of acquisition. For each probe pulse, the acquisition program takes an image and reads two digital signals that tell us if pump pulse and gas pulse are present or not

After acquiring 3000 images for each delay position between pump and probe we save the background subtracted and normalized signal

$$\frac{S(pump\&probe\&gas) - S(pump\&probe)}{S(probe\&gas) - S(probe)} \qquad (2.1)$$

where $S(pump\&probe\&gas)$ is calculated by adding up all the images that were acquired when pump, probe and gas pulses were present in the interaction region.

2.4 Results

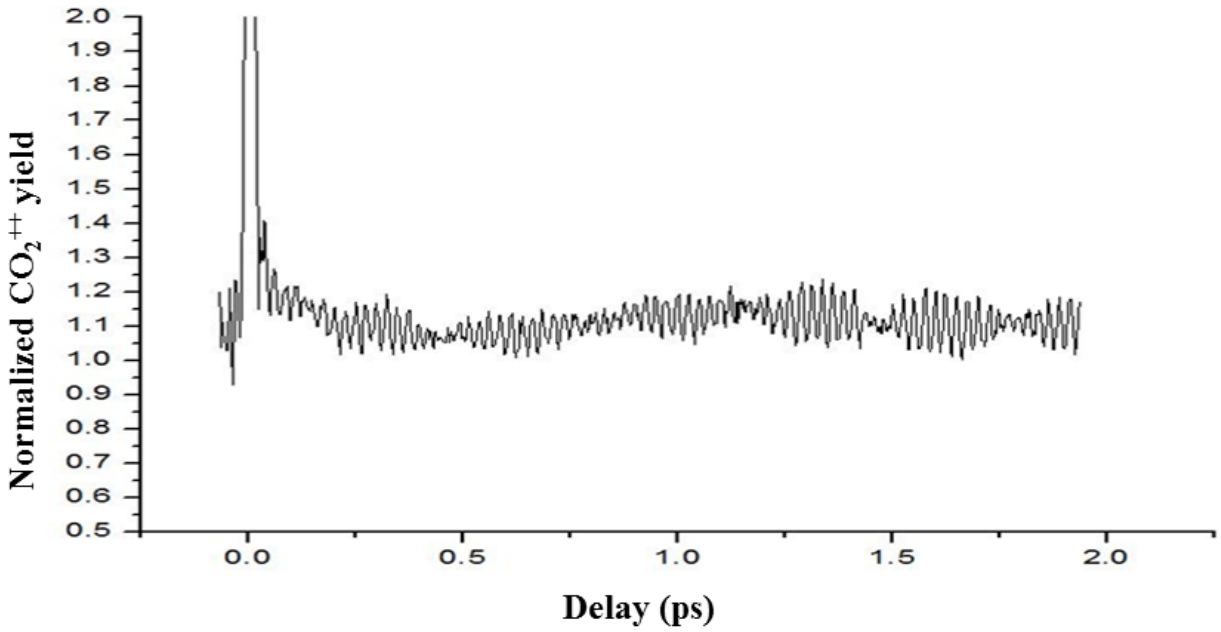

Figure 2.5 Yield of CO_2^{++} calculated according to Eq. (2.1) as a function of the delay between pump and probe.

After repeating the delay scan five times and averaging the yield acquired by Eq (2.1) at each delay point, we got the data plotted in Fig. (2.5). As we can see, the signal is modulated by different frequencies. After performing the Fourier transform of the data shown in Fig. (2.5), we can see three major peaks at 5, 38 and 41 THz. Considering Fig. (2.6) [19], which shows the electronic states of CO_2^+, it is believed that the 5 THz oscillation corresponds to the transition between the two X states of CO_2^+ [$(000)^2\Pi_{1/2} - (000)^1\Sigma^+(\tilde{X}^2\Pi_g)$] , that are split by spin-orbit

interaction. The other two frequencies, 38 THz and 41 THz have been identified as the vibrational transitions in the B $[(100) - (000)(\tilde{B}^2\Sigma_u^+)]$ and the C $[(100) - (000)(\tilde{C}^2\Sigma_g^+)]$, states of CO_2^+ [19].

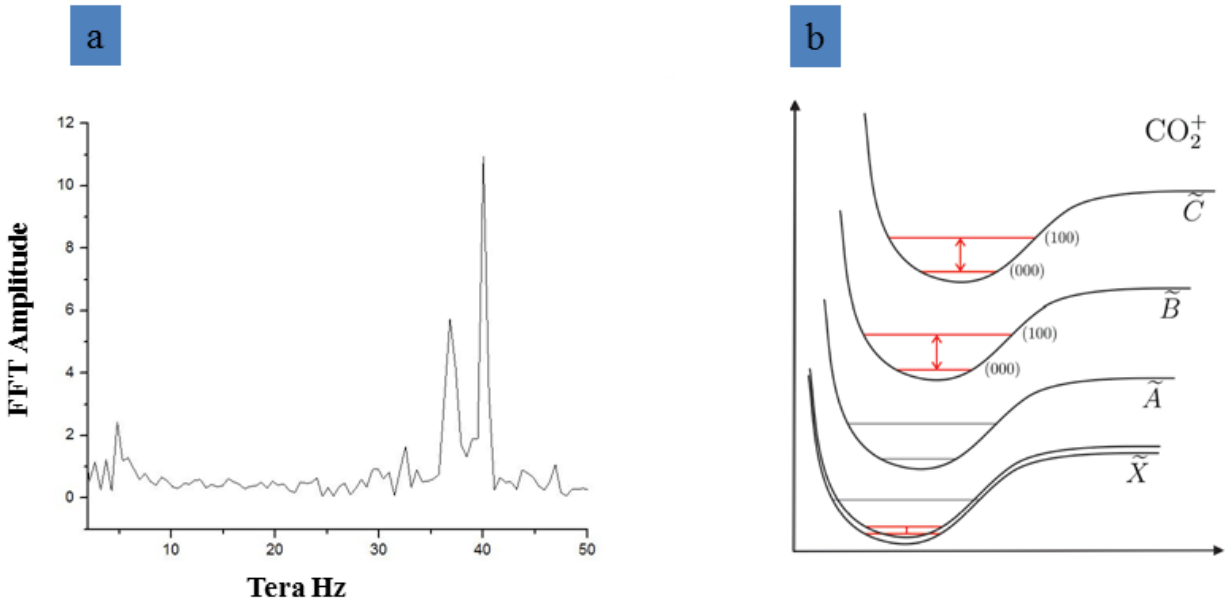

Figure 2.6 (a) Fast Fourier transform of data plotted in Fig (2.5), (b) Differet states of CO_2^+

2.5 Conclusion

By performing pump probe experiment we were able to study the ionic wave packet of CO_2^+. We saw different electronic states and corresponding vibrational states of the ion have been populated and the ionic wave packet is superposition of all these states. Due to our data acquisition, which is relatively fast, it is possible to run this experiment for different laser parameters with longer delay scans in order to learn more about the strong field ionization.

References

[1] F. Linder, M. G. Schätzel, H. Walther, A. Baltuška, E. Goulielmakis, F. Krausz, D. B. Milošević, D. Bauer, W. Becker, and G. G. Paulus, Attosecond Double-Slit Experiment, Phys. Rev. Lett. **95**, 040401 (2005).

[2] C. Ott, M. Schönwald, P. Raith, A. Kaldun, G. Sansone, M. Krüger, P. Hommelhoff, Y. Patil, Y. Zhang, K. Meyer, M. Laux, and T. Pfeifer, Strong- field spectral interferometry using the carier-envlope phase, New J. Phys. **12**, 073031 (2013).

[3] C. A. Haworth, L. E. Chipperfield, J. S. Robinson, P. L. Knight, J. P. Marangos, and J. W.G. Tisch, Half-cycle cutoffs in harmonic spectra and robust carier-envlope phase retrieval, Nature Phys. **3**, 52 (2007).

[4] L. E. Chipperfield, J. S. Robinson, P. L. Knight, J. P. Marangos, and J. W. G. Tisch, The generation and utilization of half-cycle cut-offs in high harmonic spectra, Laser Photonics Rev. **4**(6), 697 (2010).

[5] M. J. Abel, T. Pfeifer, P. M. Nagel, W. Boutu, M. J. Bell, C. P. Steiner, D. M. Neumark, and S. R. Leone, Isolated attosecond pulses from ionization gating of high-harmonic emission, J. Chem. Phys. **366**, 9 (2009).

[6] J. L. Krause, K. J. Schafer, and K. C. Kulander, High-order harmonic generation from atoms and ions in the high intensity regime, Phys. Rev. Lett. **68**, 3535 (1992).

[7] M. Lewenstein, Ph. Balcou, M. Y. Ivanov, A. L'Huillier, and P. B. Corkum, Theory of high-harmonic generation by low-frequency laser fields, Phys. Rev. A **49**, 2117 (1994).

[8] Cheng Jin, Theory of nonlinear propagation of high harmonic generation in a gaseous medium, PhD thesis, Kansas State University, 2012.

[9] V. Roudnev and B. D. Esry, General theory of carrier-envelope phase effects, Phys. Rev. Lett. **99**, 220406 (2007).

[10] Mohamad Zohrabi, Quantum control of molecular fragmentation in strong laser fields, PhD thesis, Kansas State University, 2014.

[11] O. Korilov, R. Wilcox, and O. Gessner, Nanograting-based compact vacuum ultraviolet spectrometer and beam profiler for in situ characterization of high-order harmonic generation light source, Rev. Sci. Instrum. **81**, 063109 (2010).

[12] T. Rathje, N. G. Johnson, M. Möller, F. Süßmann, D. Adolph, M. Kübel, R. Kienberger, M. F. Kling, G. G. Paulus, and A. M. Sayler, Review of attosecond resolved measurement and control via carrier-envelope phase tagging with above-threshold ionization, J. Phys. B: At. Mol. Opt. Phys. **45**, 074003 (2012).

[13] A. M. Sayler, T. Rathje, W. Müller, K. Rühle, R. Kienberger, and G. G. Paulus, Precise, real-time, every-single-shot, carrier-envelope phase measurement of ultrashort laser pulses, Opt. Lett. **36**, 1 (2011).

[14] Xiaoming Ren, Laser-driven rotational dynamics of gas-phase molecules: control and application, PhD thesis, Kansas State University, 2013.

[15] P. Rudawski, A. Harth, C. Guo, E. Lorek, M. Miranda, C. M. Heyl, E. W. Larsen, J. Ahrens, O. Prochnow, T. Binhammer, U. Morgner, J. Mauritsson, A. L'Huillier, and C. L. Arnold, Carrier-envlope phase dependent high-order harmonic generation with a high-repetition rate OPCPA-system, Eur. Phys. J. D **69**, 70 (2015).

[16] H. Timmers, Z. Li, N. Shivaram, R. Santra, O. Vendrell, and A. Sandhu, Coherent electron hole dynamics near a conical intersection, Phys. Rev. Lett. **113**, 113003 (2014).

[17] P. M. Kraus, S. B. Zhang, A. Gijsbertsen, R. R. Lucchese, N. Rohringer, and H. J. Wörner, High-harmonic probing of electronic coherence in dynamically aligned molecules, Phys. Rev. Lett. **111**, 243005 (2013).

[18] O. Smirnova, Y. Mairesse, S. Patchkovskii, N. Dudovich, D. Villeneuve, P. Corkum, and M. Y. Ivanov, High harmonic interferometry of multi-electron dynamic in molecules, Nature **460**, 972 (2009).

[19] Markus Schürholz, Pump-Probe Experimente an Molekülen mit intensiven Laserpulsen, Diploma thesis, Heidelberg University, 2009.

[20] A.T.J.B. Eppink, and D.H. Parker, Velocity map imaging of ions and electrons using electrostatic lenses: Application in photoelectron and photofragment ion imaging of molecular oxygen, Rev. Sci. Instrum. **68**, 3477 (1997).

[21] Varun Makhija, Laser-induced rotational dynamics as a route to molecular frame measurements, PhD thesis, Kansas State University, 2014.